

†Electronic Supplementary Information

**An efficient cocatalyst of defects-decorated MoS₂ ultrathin
nanoplate for promotion of photocatalytic hydrogen evolution
over CdS nanocrystal**

Jinhua Xiong, Yuhao Liu, Dengke Wang, Shijing Liang, Weiming Wu,
Ling Wu*

State key laboratory of photocatalysis on energy and environment, Fuzhou University,

Fuzhou 350002, P. R. China

* Corresponding author: Ling Wu

E-mail: wuling@fzu.edu.cn

Phone: +86-591-83779362

Fax: +86-591-83779105

Experiment details

Synthesis of defect-rich MoS₂ ultrathin nanoplate: 79 mg ammonium molybdate (NH₄)₆Mo₇O₂₄ · 4H₂O) was dissolved in 25 ml N-N'-dimethyl formamide (DMF) contained in a 100 mL Teflon-line stainless steel autoclave. Then, 150 mg thiourea was added into the autoclave. Subsequently, the autoclave was sealed and maintained at 200 ° C for 24 h and then allowed to cool to room temperature. A black precipitate was collected and washed with deionized water and absolute ethanol. The final products were dried in an oven at 60 ° C for 12 h.

Synthesis of defect-free MoS₂ ultrathin nanoplate: 1mmol ammonium molybdate (NH₄)₆Mo₇O₂₄ · 4H₂O) and 30 mmol thiourea was dispersed in 35 ml deionized water contained in a 100 mL Teflon-line stainless steel autoclave. After stirring for an hour, the autoclave was sealed and maintained at 220 ° C for 24 h and then allowed to cool to room temperature. A black precipitate was collected and washed with deionized water and absolute ethanol. The final products were dried in an oven at 60 ° C for 12 h.

Note: In fact, the obtained defect-free MoS₂ ultrathin nanoplate is not without any defect. Compared with the defect-rich MoS₂-NS, its defects can be ignored. For convenience, we called it defect-free MoS₂ ultrathin nanoplate.

Synthesis of CdS/MoS₂ ultrathin nanoplate composition: a certain amount of the resulted MoS₂-NS (8, 12 and 16 mg corresponding to 10%, 15% and 20%, respectively) was dispersed in 150 ml deionized water by ultrasound for 2 h. Subsequently, 27.7 mmol⁻¹ CdCl₂ aqueous solution (20 ml) was added into the mixture, stirring vigorously for another 1 h. Then, addition of 14 mmol⁻¹ Na₂S aqueous solution (40 ml) was added into the mixture drop by drop under vigorous stirring. After that, the mixture was kept stirring for 1h. Finally, the mixture was standing for 30 mins and the sediment was collect and washed with deionize water. The final products were dried in vacuum at 60 ° C for 12 h.

Preparation of mechanical mixture of CdS and MoS₂-NS: the as-prepared MoS₂-NS was added into the Commercial CdS or home-made CdS aqueous suspension directly, which was designed as “C-CdS+MoS₂-NS” and “B-CdS+MoS₂-NS”, respectively, in the manuscript.

Characterization

X-ray diffraction (XRD) patterns were recorded on a Bruker D8 Advance X-ray diffractometer with Cu K α irradiation operated at 40 kV and 40 mA. The data were recorded in a 2θ range of 5–70° with a step width of 0.01°. Hitachi New Generation SU8010 Field-emission scanning electron microscopy (FESEM) was used to determine the morphology of the samples. Transmission electron microscopy (TEM), high-resolution (HR) TEM images, selected area electron diffraction (SAED) and

energy-dispersive X-ray spectroscopy (EDX) were obtained on a FEI Tencai 20 transmission electron microscope at an accelerating voltage of 200 kV. UV-vis diffuse reflectance spectra (UV-vis DRS) were obtained by a UV-vis spectrophotometer (Varian Cary 500). The Brunauer–Emmett–Teller (BET) surface area was measured with an ASAP2020M apparatus (Micromeritics Instrument Corp). Electron Paramagnetic resonance (EPR) signals were recorded with a Bruker A300 spectrometer. Raman spectra were collected via a multichannel modular triple Raman system (Renishaw Co.) with confocal microscope at room temperature using the 532 nm laser. X-ray photoelectron spectroscopy (XPS) measurements were performed on a PHI Quantum 2000 XPS system with a monochromatic Al K α source and a charge neutralizer. The XAFS data at the Mo K-edge of the samples were recorded at room temperature in transmission mode using ion chambers at beam line BL14W1 of the Shanghai Synchrotron Radiation Facility (SSRF), China. The station was operated with a Si(111) double crystal monochromator. During the measurement, the synchrotron was operated at energy of 3.5 GeV and a current between 150-210 mA. The photon energy was calibrated with the first inflection point of Mo K-edge in Mo metal foil.

Electrochemical measurements

Electrochemical measurements were performed in a three-electrode system at an electrochemical station (CHI660E). Typically, 4 mg of sample and 40 μ l nafion were dispersed in 1 ml water-ethanol (4:1, volume ratio) solution by sonicating for at least 2 h to form a homogeneous ink. 5 μ l of the dispersion was loaded onto a glassy carbon electrode with 3 mm diameter. Linear sweep voltammetry was carried out in 0.5 M H₂SO₄ (purged with high-purity Ar) with scan rate of 10 mV s⁻¹ using saturated calomel electrode (SCE), a graphite rod and the glassy carbon electrode as the reference electrode, counter electrode and working electrode, respectively. The Nyquist plots were recorded with frequencies ranging from 100 kHz to 10 Hz at an amplitude of 500 mV.

Photocatalytic Test

The photocatalytic reactions were carried out in a Pyrex reaction cell connected to a closed gas circulation and evacuation system. 80 mg photocatalyst was suspended in 80 mL of (0.02 M) SO₃²⁻ / (0.1 M) S²⁻ aqueous solution. The suspension was then thoroughly degassed and irradiated by a 300 W Xenon lamp (PLS-SXE300C, Perfectlight Co., Beijing) with a cut off filter of 420 nm. H₂ is detected by an online gas chromatograph.

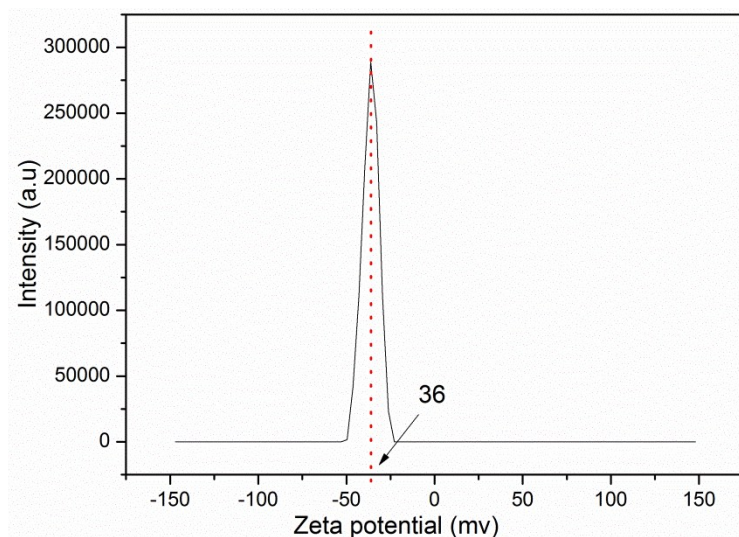


Fig. S1 Zeta potential of the MoS₂-NS dispersed in deionized water

As shown in Fig. S1 the as-prepared MoS₂-NS has a zeta-potential (ξ) value of -36 mV, which makes it possible for Cd²⁺ to adsorb on the MoS₂-NS via electrostatic interaction.

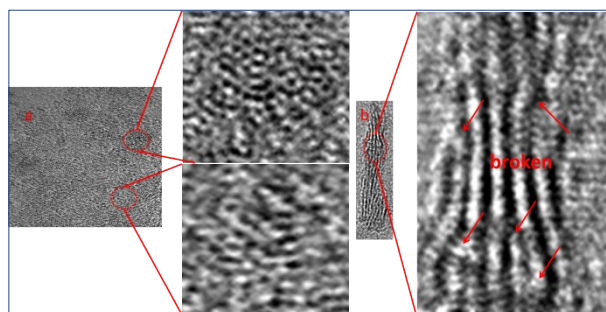


Fig. S2a and b) amplification of the HRTEM image in Fig. 1C and Fig. 1D, respectively.

As shown in Fig. S2a-b, many disordered structure are observed in the basal plane of the MoS₂ ultrathin nanoplate. Furthermore, discontinuous and terminational S-Mo-S slabs are also observed.

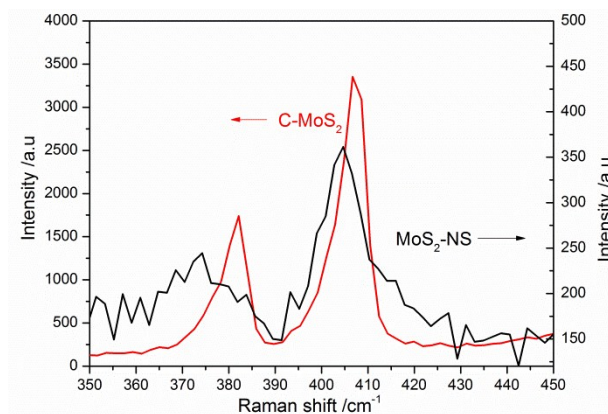


Fig. S3 Raman spectra of the C-MoS₂ and the as-prepared MoS₂-NS

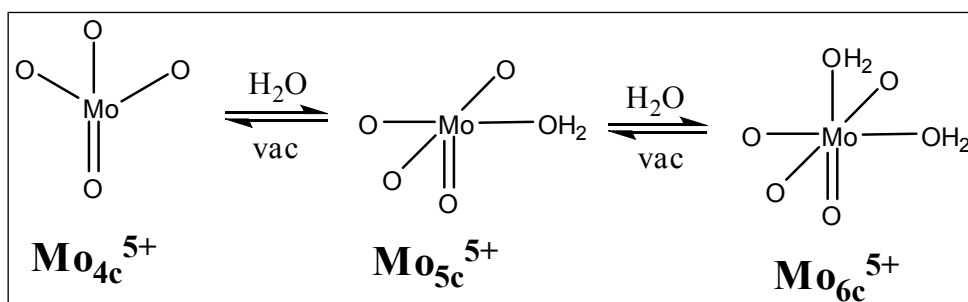


Fig. S4 change in the three Mo⁵⁺ coordination sphere during water adsorption

It's reported that the coordination sphere of the three Mo⁵⁺ can be changed reversibly during water adsorption.¹ Although the Mo⁵⁺ and the Mo-O bond were detected by XPS and EPR, unfortunately, it's unclear to know the coordination mode of the Mo⁵⁺ in the MoS₂ ultrathin nanoplate. It's well known that the investigation on the defects of MoS₂ for HER is still a big challenge. However, something is certain that the existence of Mo⁵⁺ benefits the hydrogen production, which may provide with guidance for the engineering of the defect of MoS₂ for HER.

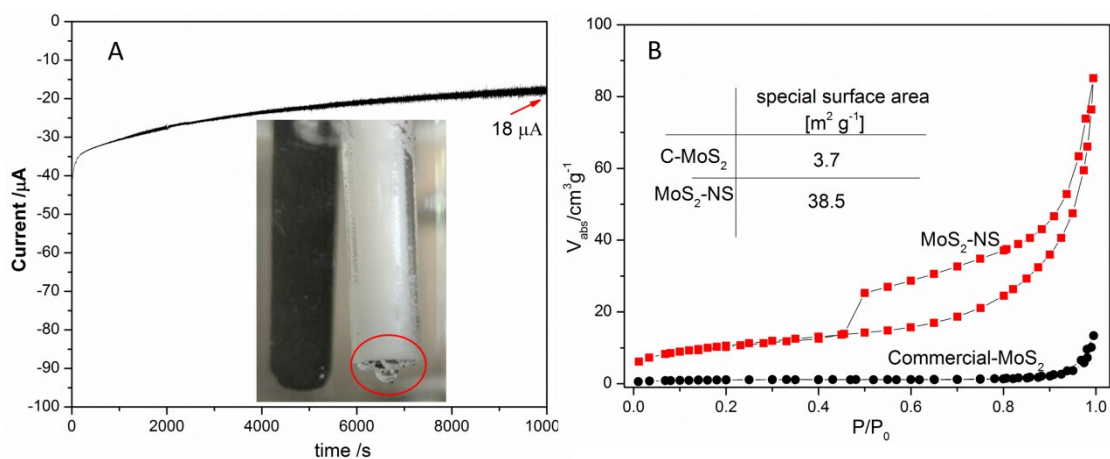


Fig. S5 A) Time dependence of current under static potential of -0.45 V (vs. SCE). Inset: photo of the hydrogen bubbles generated from the glassy carbon working electrode during the test. B) BET adsorption-desorption isotherm of C-MoS₂ and MoS₂-NS

As shown in Fig. S5A, a continuous cathode current for HER was observed under the constant potential of -0.45 V. Hence it is reasonable to consider that the onset potential for HER is -0.4 V on account of the occurrence of current around -0.4 V (showing in Fig. 3B in the manuscript). Fig. S5B demonstrates that the as-prepared MoS₂-NS has a large special surface area (38.5 m²/g), which is about 10 times higher than that of the Commercial MoS₂, because of the ultrathin two-dimensional features.

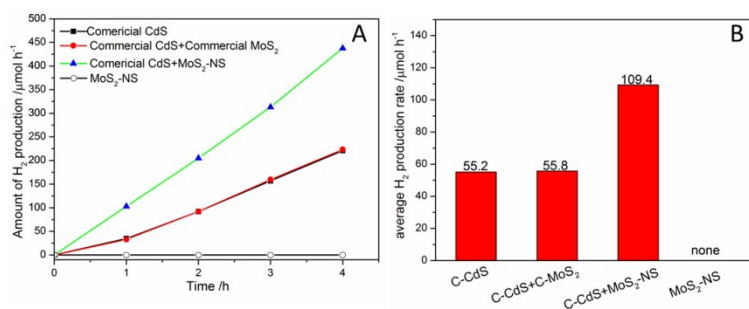


Fig. S6A and B) time course of H₂ evolution over different photocatalyst and the corresponding average H₂ production rate, respectively.

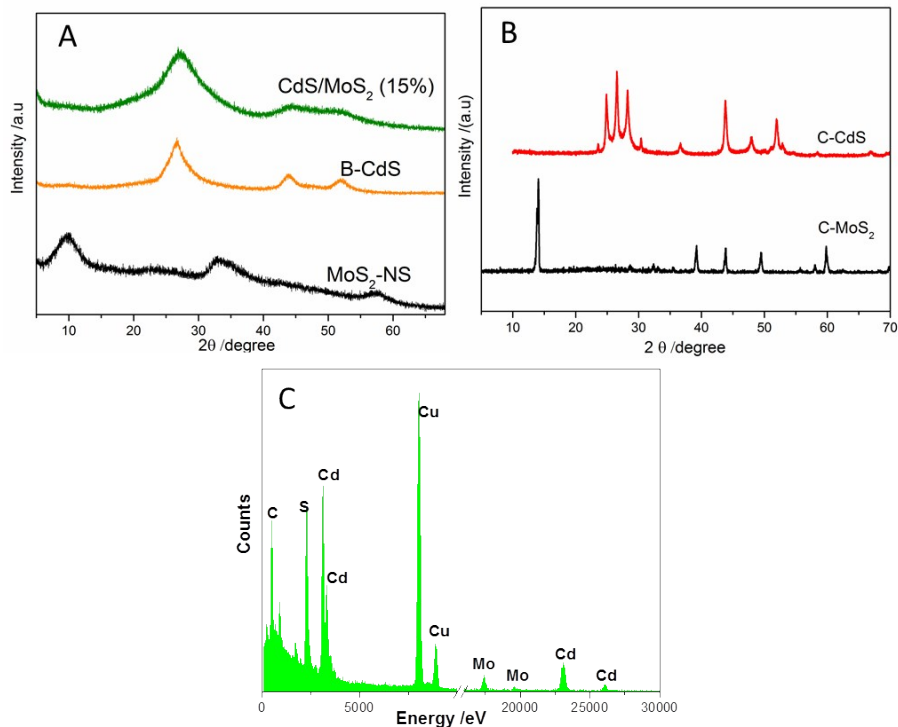


Fig. S7 the XRD patterns of the samples

As shown in Fig. S7A, the XRD patterns of the resulted CdS/MoS₂ just shows the diffraction peak of the CdS due to the weak diffraction peak of MoS₂ covered by that of CdS. Fig. S7B shows the XRD patterns of the C-CdS and C-MoS₂. Based on the calculation of Bragg equation, the interlayer spacing of the (002) plane of C-MoS₂ is 0.62 nm. Fig. S7C is the EDX spectra of the resulted CdS/MoS₂ (15%).

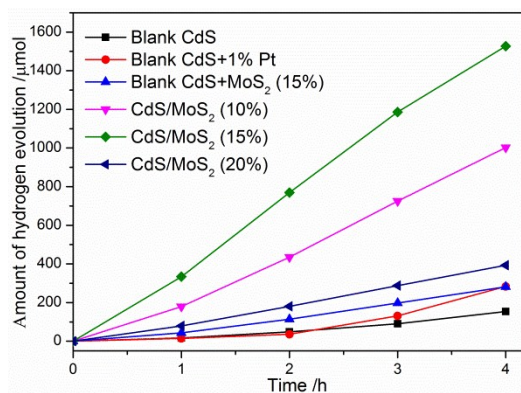


Fig. S8 time course of H₂ evolution over the as-prepared samples.

As shown in Fig. S8, the CdS/MoS₂ composition show a better photocatalytic H₂ evolution than the blank CdS, CdS/Pt(1%) and the mechanical mixture (CdS+MoS₂-NS), arising from the synergetic effect of MoS₂-NS. As shown in Fig. S9, the B-CdS tend to aggregate without the MoS₂-NS as the platform for nucleation. Additionally, the photocatalytic activity of CdS/MoS₂ varies with the incremental dosage of MoS₂-NS because of the shield effect of the MoS₂-NS. Here, 15% of the MoS₂-NS is considered to be the optimal content in CdS/MoS₂ system.

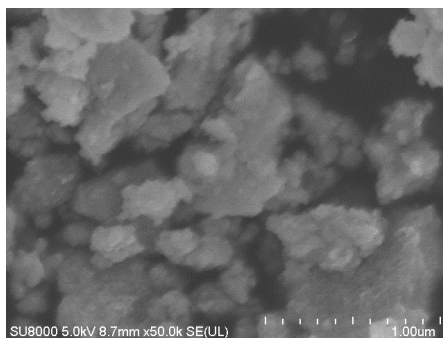


Fig. S9 FESEM images of the blank CdS

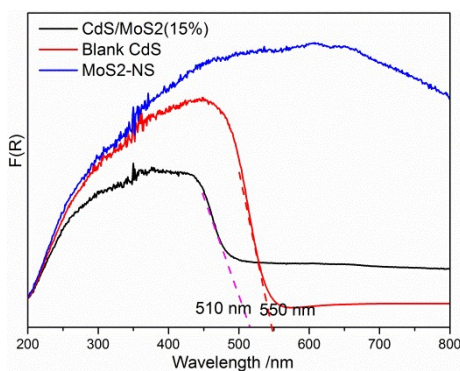


Fig. S10 UV-vis DRS spectra of the as-prepared samples.

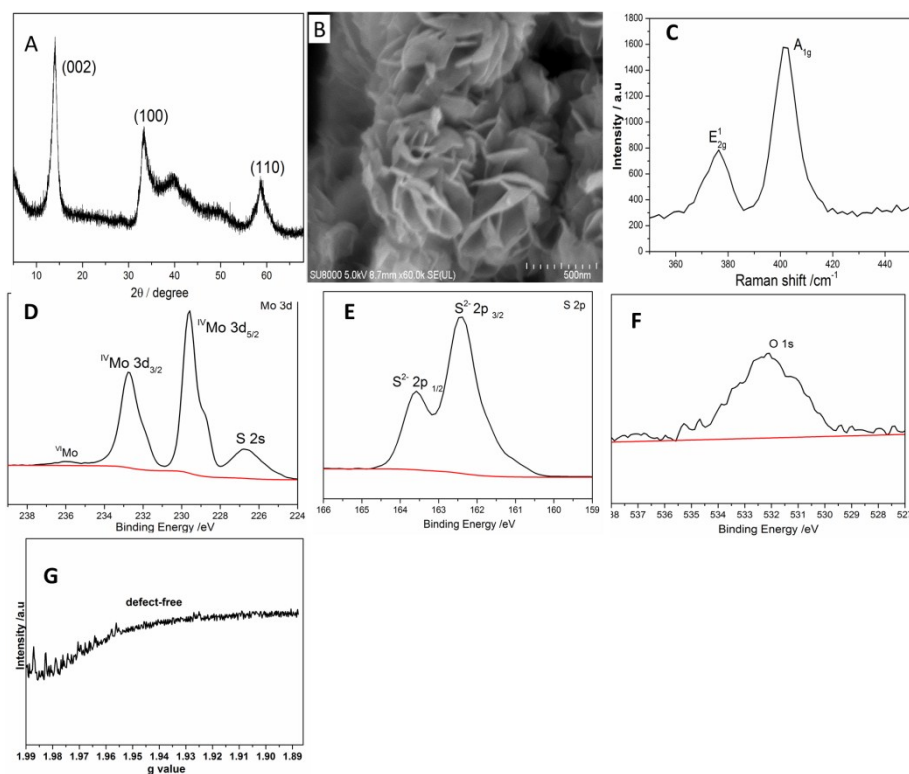


Fig. S11 A-C) the XRD patterns, the SEM images and the Raman spectra of the defect-free MoS₂ ultrathin nanoplate; D-F) XPS spectra of Mo 3d, S 2p and O 1s, respectively; G) EPR spectra recorded at 77k

As shown in Fig. S11, the XRD patterns have a distinct difference with the defect-rich MoS₂. That is, the diffraction peak of the (002) plane of the MoS₂ comes back to 14.0°, consistent with that of the C-MoS₂. Additionally, the stronger and sharper XRD diffraction patterns and the Raman spectra than that of the defect-rich MoS₂ ultrathin nanoplate indicate that the superior crystallization than the defect-rich MoS₂ ultrathin nanoplate. More interestingly, the XPS spectra of the Mo 3d and the S 2p of the defect-free MoS₂ ultrathin nanoplate didn't detect the Mo⁵⁺ and S₂²⁻, respectively. Furthermore, the spectra of O 1s demonstrated trace oxygen was introduced into the lattice of the MoS₂. Additionally, the Mo⁵⁺ signal is also lost in EPR spectra along with the disappearance of defects. Hence, it's reasonable to believe that the defective site is where the unsaturated Mo and S₂²⁻ are formed. Furthermore, it's well known that the S₂²⁻ is a kind of steady active site for hydrogen production.² However, the unsaturated Mo will suffer from oxidation in the O₂-rich condition, leading to the formation of Mo⁵⁺-O. Significantly, the bonding between Mo and O contributes to a positive effect on the conductivity and expand the interlayer space of (002) plane.^{3,4} Under these synergic effects, the defect-rich MoS₂ ultrathin nanoplate demonstrates an excellent promotion for hydrogen production.

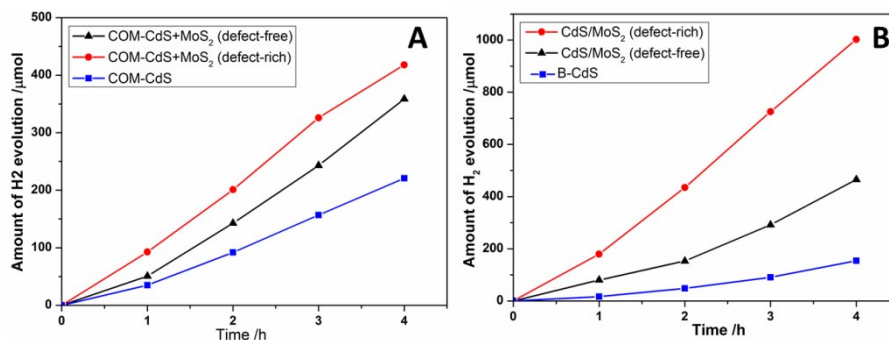


Fig. S12A and B) the time course of H₂ evolution over the C-CdS+MoS₂ (10%) and CdS/MoS₂ (10%), respectively. Defect-rich MoS₂ ultrathin nanoplate (red); defect-free MoS₂ ultrathin nanoplate (black).

As shown in Fig. S12, the defect-rich MoS₂ ultrathin nanoplate shows a better promotion for the photocatalytic hydrogen evolution over CdS nanocrystals than the defect-free MoS₂ ultrathin nanoplate, demonstrating that the defects are the active site for hydrogen production.

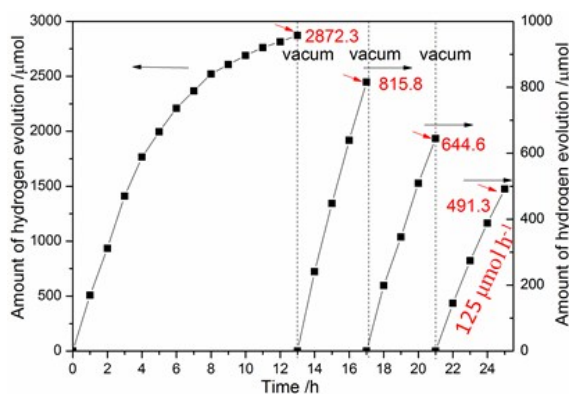


Fig. S13 time course of H₂ evolution over the CdS/MoS₂ (15%).

Turnover number (TON)= (the number of reaction electron) / (per number of photocatalyst molecules)

$$TON = \frac{(2872.3 + 815.8 + 644.6 + 491.3 * 2) / 1000}{80 * 85\% / 144.5} = 20.5$$

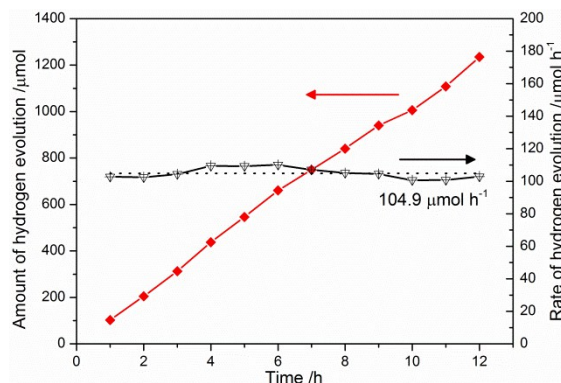


Fig. S14 time course of H₂ evolution over the CdS+MoS₂ (15%) (red) and the corresponding average H₂ evolution rate (black).

Note: The photocatalytic stability of the C-CdS shows better than that of the CdS nanocrystal, which is attributed to the superior crystallinity of the C-CdS. But the photocorrosion of the C-CdS is also inevitable after a longer reaction time.

Reference

1. C. Louis and M. Che, *J. Phys. Chem.*, 1987, **91**, 2875-2883
2. C. Tsai, F. Ablid-Pedersen, J. K. Nørskov, *Nano lett.*, 2014, **14**, 1381-1387
3. J. Xie, J. Zhang, S. Li, F. Grote, X. Zhang, H. Zhang, R. Wang, Y. Lei, B. Pan and Y. Xie, *J. Am. Chem. Soc.*, 2013, **135**, 17881-17888
4. H. Nan, Z. Wang, W. Wang, Z. Liang, Y. Lu, Q. Chen, D. He, P. Tan, F. Miao, X. Wang, J. Wang and Z. Ni, *ACS Nano*, 2014, **8**, 5738-5745.